Physics Letters A 372 (2008) 4532–4535

Contents lists available at ScienceDirect

Physics Letters A

www.elsevier.com/locate/pla

Multiple omnidirectional resonances in a metamaterial sandwich

Jian-Wen Dong, Kai-Shun Wu, Cong Mu, He-Zhou Wang *

State Key Laboratory of Optoelectronic Materials and Technologies, Zhongshan (Sun Yat-Sen) University, Guangzhou 510275, China

ARTICLE INFO

Article history:
Received 8 November 2007
Received in revised form 2 April 2008
Accepted 9 April 2008
Available online 16 April 2008
Communicated by R. Wu

PACS:
41.20.Jb
78.20.Ci
42.81.-I
42.79.Ci

Keywords:
Film
Negative index material
Filters

ABSTRACT

Multiple omnidirectional resonances are found in a sandwich structure consisting of a left-handed metamaterial cavity and two single-negative-permittivity reflection walls. These resonances appear because the phase shift of left-handed metamaterial can cancel the reflection phase shift of single-negative-permittivity metamaterials at every incidence angle. By using such particular structure, a kind of structure possessing multiple omnidirectional resonances in both polarizations has been designed. In addition, issues associated with energy loss are discussed.

1. Introduction

As we know, the cavity modes appear in defective photonic crystals due to the breakdown of translation invariance in periodic systems. Their unique properties have brought up many applications in communications and localizations. But these cavity modes are restricted by the size of the defect and the incidence electromagnetic (EM) wave. For example, in photonic crystal structures consisting of only positive-index materials (both positive permittivity and permeability), with the increase of the defect thickness and the incidence angle, the resonant frequencies will always blueshift [1–3], which limits their applications. In order to overcome it, several kinds of structures consisting of metal [4] or metamaterial [5–9] have been proposed. It is shown that when the effective parameters of metamaterials satisfy the near-zero dispersion condition, the resonant frequencies are nearly unchanged in different tangential wavevector. It is called omnidirectional resonance (ODR) [10–12]. However, all the structures above are single ODR channel. The structure with multiple ODR channels has never been reported. Furthermore, except Ref. [4], all the structures above are based on the photonic band gap effect. It requires a large number of periodicity to form the bandgap, leading to the disadvantage for fabrications and integrations.

Metamaterial is a kind of man-made materials. The remarkable benefit on metamaterial is that its effective parameters may be engineered artificially to meet various needs. One of the most prominent cases is that one can utilize metamaterials to accomplish the invisible cloak by tuning the effective permittivity and permeability in the range between zero and one [13]. Moreover, different kinds of the metamaterials have different dispersion relationships. For example, a metamaterial has Drude dispersion when it is realized by distributed L–C transmission lines [6–8]. Therefore, it is possible to achieve multiple ODRs by using some special metamaterials.

In this Letter, a sandwich structure, consisting of epsilon-negative/left-handed/epsilon-negative (ELE) metamaterials geometry, is studied. One or multiple ODR modes for both polarizations are found in this symmetric structure. These findings will lead to potential applications.

2. Dispersion on cavity mode

The geometry of the system under study is shown in Fig. 1(a). The slabs (denoted by "1") at both sides are epsilon-negative material (ENG), while the middle slab (denoted by "2") is a left-handed material (LHM) with the thickness of $2d$. We use the Drude model to describe the isotropic materials, that is,

$$\varepsilon_j = \varepsilon_{0j} - \frac{\omega_{ep,j}^2}{\omega^2}, \qquad \mu_j = \mu_{0j} - \frac{\omega_{mp,j}^2}{\omega^2}, \quad j = 1, 2, \tag{1}$$

* Corresponding author. Tel.: +86 20 84113679; fax: +86 20 84037423.
E-mail address: stswhz@mail.sysu.edu.cn (H.-Z. Wang).

0375-9601/$ – see front matter
doi:10.1016/j.physleta.2008.04.024

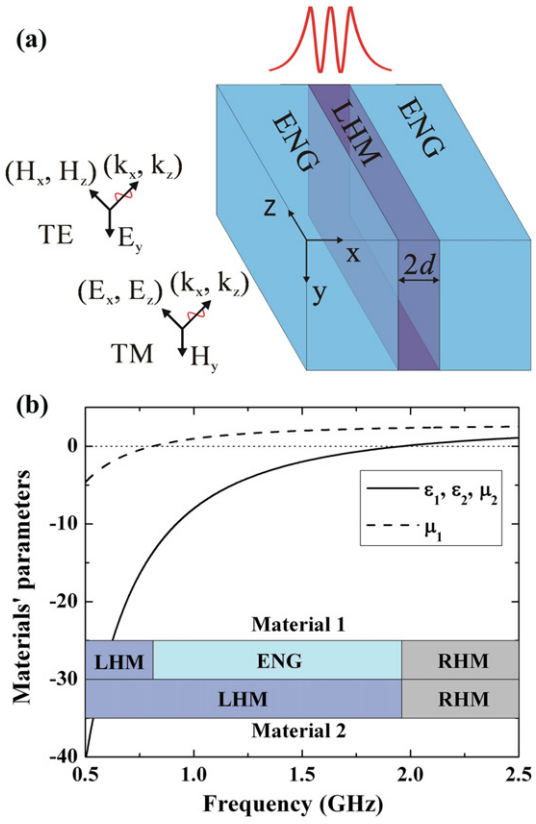

Fig. 1. (Color online.) (a) Illustration of the symmetric ELE sandwich. (b) The relationships between the frequency and the materials' effective parameters.

where ε_{0j} (μ_{0j}) and $\omega_{ep,j}$ ($\omega_{mp,j}$) are the effective static electric (magnetic) constants and the effective electric (magnetic) plasma frequencies, respectively. Here, we choose $\varepsilon_{0j} = \mu_{0j} = 2.828$, $\omega_{ep,j}^2 = \omega_{mp,2}^2 = 428.8\ \text{GHz}^2$, and $\omega_{mp,1}^2 = 73.6\ \text{GHz}^2$, which can be realized in artificial designed transmission lines [6–8]. It is clearly shown in Fig. 1(b) that ε_1, ε_2 and μ_2 are equally dependent on the frequency. As the frequency range of ENG in material 1 is from 0.812 to 1.96 GHz, and LHM in material 2 is below 1.96 GHz, the frequency range from 0.812 to 1.96 GHz is of our interest. Note that the assumption $\varepsilon_1 = \varepsilon_2 = \mu_2$ is just for simplification, and is not necessary for the following discussions.

In fact, the ELE structure can be regarded as a one-dimensional microcavity of finite thickness ($2d$). The EM wave propagates in the LHM and decays exponentially in the ENG. The structure always supports two kinds of cavity modes: one is the symmetrical (S) mode that has even field distribution; another is the antisymmetrical (AS) mode that has odd distribution. For the transverse electric (TE) mode, the fields have the forms of:

$$E_y = \begin{cases} A\{{}^{\cos}_{\sin}\}(k_2 x)\exp(i\beta z), & |x| \leqslant d, \\ B\exp(-\alpha_1|x|)\exp(i\beta z), & |x| \geqslant d, \end{cases} \tag{2}$$

$$H_x = -\frac{i}{\omega\mu_j}\frac{\partial}{\partial z}E_y = \begin{cases} (-\frac{\beta A}{\omega\mu_2})\{{}^{\cos}_{\sin}\}(k_2 x)\exp(i\beta z), & |x| \leqslant d, \\ -\frac{\beta B}{\omega\mu_1}\exp(-\alpha_1|x|)\exp(i\beta z), & |x| \geqslant d, \end{cases} \tag{3}$$

$$H_z = -\frac{i}{\omega\mu_j}\frac{\partial}{\partial x}E_y = \begin{cases} (i\frac{k_2 A}{\omega\mu_2})\{{}^{-\sin}_{+\cos}\}(k_2 x)\exp(i\beta z), & |x| \leqslant d, \\ i\frac{\alpha_1 B}{\omega\mu_1}\operatorname{sgn}(x)\exp(-\alpha_1|x|)\exp(i\beta z), & |x| \geqslant d, \end{cases} \tag{4}$$

where $\alpha_1 = \sqrt{\beta^2 - \varepsilon_1\mu_1\omega^2/c^2}$, $k_2 = \sqrt{\varepsilon_2\mu_2\omega^2/c^2 - \beta^2}$; β is the z component of wavevector; ω and c are the angular frequency and light speed in vacuum; A and B are the connected coefficients. In the first formula of Eqs. (2)–(4), the upper (lower) line corresponds to the S (AS) mode. Continuity of E_y and H_x at each interface yields the cavity mode dispersion relations:

$$\left(\frac{k_2}{\mu_2}\right)\left\{{}^{-\tan}_{+\cot}\right\}(k_2 d) + \frac{\alpha_1}{\mu_1} = 0. \tag{5}$$

On the other hand, for the transverse magnetic (TM) mode, the fields have the forms of,

$$H_y = \begin{cases} A\{{}^{\cos}_{\sin}\}(k_2 x)\exp(i\beta z), & |x| \leqslant d, \\ B\exp(-\alpha_1|x|)\exp(i\beta z), & |x| \geqslant d, \end{cases} \tag{6}$$

$$E_x = -\frac{i}{\omega\varepsilon_j}\frac{\partial}{\partial z}H_y = \begin{cases} (\frac{\beta A}{\omega\varepsilon_2})\{{}^{\cos}_{\sin}\}(k_2 x)\exp(i\beta z), & |x| \leqslant d, \\ \frac{\beta B}{\omega\varepsilon_1}\exp(-\alpha_1|x|)\exp(i\beta z), & |x| \geqslant d, \end{cases} \tag{7}$$

$$E_z = \frac{i}{\omega\varepsilon_j}\frac{\partial}{\partial x}H_y = \begin{cases} (i\frac{k_2 A}{\omega\varepsilon_2})\{{}^{-\sin}_{+\cos}\}(k_2 x)\exp(i\beta z), & |x| \leqslant d, \\ -i\frac{\alpha_1 B}{\omega\varepsilon_1}\operatorname{sgn}(x)\exp(-\alpha_1|x|)\exp(i\beta z), & |x| \geqslant d \end{cases} \tag{8}$$

and the dispersion relation is:

$$\left(\frac{k_2}{\varepsilon_2}\right)\left\{{}^{-\tan}_{+\cot}\right\}(k_2 d) + \frac{\alpha_1}{\varepsilon_1} = 0. \tag{9}$$

One can find that the dispersion relations between TE mode [Eq. (5)] and TM mode [Eq. (9)] have the same forms except $\mu_j \leftrightarrow \varepsilon_j$. In other words, the dispersion is mainly determined by materials' permeability and permittivity in TE and TM mode, respectively. We also note that α_1 and k_2 must be real to ensure the propagating (decaying) field pattern in the cavity (walls).

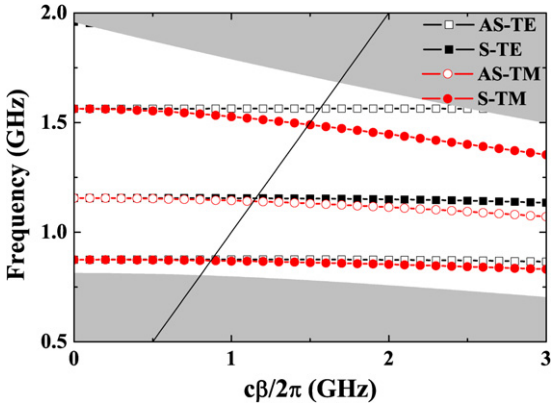

Fig. 2. (Color online.) Dispersions on an ELE structure with the LHM thickness of 31.95 mm. The square (circle) symbols stand for the TE (TM) mode. The solid (open) symbols stand for the S (AS) mode. The thin solid line is the light line.

3. Results and discussions

By using Eq. (5), the dispersion of both TE and TM modes are investigated. Here, we first choose the thickness of LHM to be 31.95 mm. It has three TE and three TM modes. According to the symmetry and node of field patterns, from high to low frequency, TE modes can be denoted as AS-TE1, S-TE2, and AS-TE3, while TM modes can be denoted as S-TM0, AS-TM1 and S-TM2. The dispersion is shown in Fig. 2. It is found that at normal incidence ($\beta = 0$), TE and TM modes are degenerate, but have opposite symmetries. Moreover, at small-angle incidence, the modes for both polarizations are almost overlapped. However, at large-angle incidence and outside the light line, they exhibit different dispersions. Some of them (e.g., the S-TM0 mode) have large negative dispersion while some (e.g., the S-TE mode) are nearly angular independence, i.e., ODR. Interestingly, these ODR modes are inside

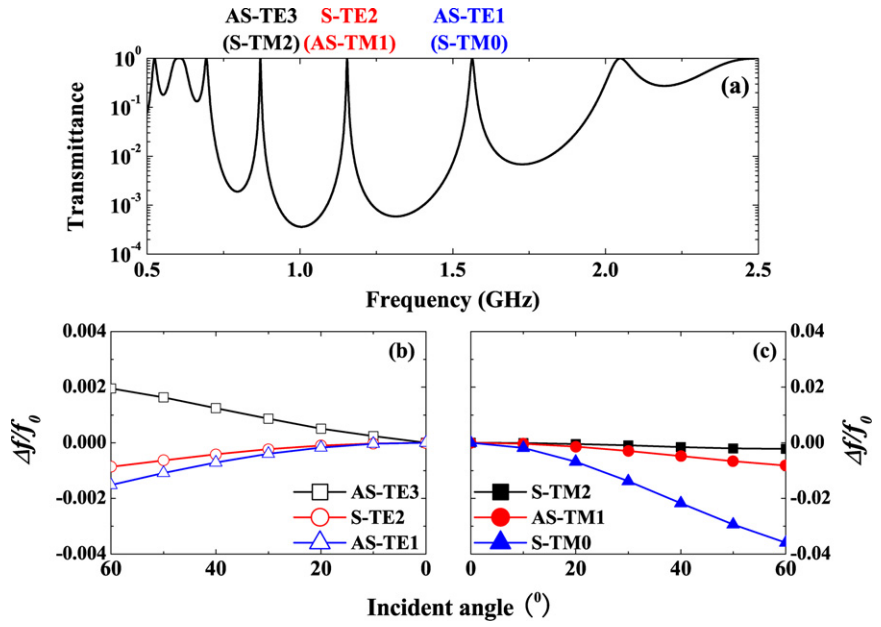

Fig. 3. (Color online.) (a) Transmission spectrum of an ELE structure in which the thicknesses of three layers are 31.95 mm. (b) and (c) are the dependence of the TE and TM mode on the incidence angle. Here, $\Delta f = f - f_0$ (f_0 is the resonant frequency of each mode at normal incidence). Note that the range of vertical axis in (c) is ten times larger than that in (b).

the light line, which may be coupled by the externally incidence EM wave if the ENG walls are of finite thickness.

To demonstrate this, we have calculated an ELE structure with finite ENG walls using the transfer matrix method. All layers are 31.95 mm thick. Fig. 3(a) is the transmission spectrum at normal incidence. Fig. 3(b) and (c) are the angular dependences of TE and TM modes on the incidence angle. It is shown that the frequency shift is positive for the AS-TE3 mode; while the shifts are negative for the AS-TE1, S-TE2, and all TM modes. Moreover, except the S-TM0 mode, the resonant frequencies of other modes shift only on the order of a thousandth, which exhibit ODR properties.

The physical reason of ODRs can be explained by considering the phase matching between the reflected wave from the ENG and the propagating wave of the LHM. Take TE mode for example. The phase shift of reflection coefficient at the interface between the LHM and ENG is [14]:

$$\phi_{\text{ref}} = -2\,\text{atan}\left(\frac{\sqrt{\mu_2}\sqrt{\varepsilon_2\mu_2\sin^2\theta_2 - \varepsilon_1\mu_1}}{\sqrt{\varepsilon_2}\mu_1\cos\theta_2}\right), \tag{10}$$

where $\sin\theta_2 = \sin\theta_0/(\sqrt{\varepsilon_2}\sqrt{\mu_2})$; θ_0 is the incidence angle. Meanwhile, the propagating phase shift in the LHM is

$$\phi_{\text{prop}} = 4\pi f d\sqrt{\varepsilon_2}\sqrt{\mu_2}\cos\theta_2/c. \tag{11}$$

The total phase shift ϕ_{tot} is the summation of ϕ_{ref} and ϕ_{prop}. If $\phi_{\text{tot}} = n\pi$ (n is integer) is satisfied, the propagating phase shift in the LHM can totally cancel the reflection phase shift of the ENG on each cycle. As a result, the resonance will appear. Fig. 4 is the contour diagram of ϕ_{tot} at different frequency and different incidence angle for the TE mode. It is found that the contours of $\phi_{\text{tot}} = n\pi$ are almost horizontal. This indicates the resonant frequencies are almost the same at every angle. The transmission peaks extracted by transfer matrix method are also plotted in Fig. 4 (open-circle) for demonstration. It can be seen that the locations of these peaks are just on the contours of $\phi_{\text{tot}} = n\pi$.

Next, we study the dependence of ODR modes on the cavity thickness. Fig. 5(a) is the contour diagram of the frequency for the AS-TE3 mode at different thickness and tangential wavevector. It

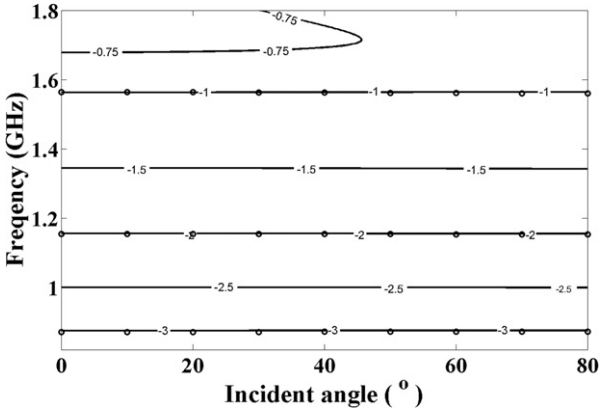

Fig. 4. Contour diagram (solid lines) of total phase shift (in unit of π). The ELE structure is the same as Fig. 2. The open-circles are the transmission peaks extracted from Fig. 3(b). Note that all the circles are at the lines $n\pi$, satisfying the phase matching condition at every incidence angle.

is found that around 0.85–1.1 GHz, the contours are almost horizontal again. Further calculations show that the contours of other high order TE and TM modes are also horizontal. This indicates that in this frequency range, the phase matching appears in various TE and TM modes simultaneously, leading to multiple ODRs. In Fig. 5(b), with the cavity thickness of $2d = 95.85$ mm, three transmission peaks in the lower frequency range exhibit all-polarized ODRs. In fact, more and more ODR peaks will appear with the increasing of the LHM thickness due to the cavity effect. Fig. 6 shows the dependence between the resonant frequencies and LHM thickness. Indeed, we can find that the number of ODRs increases with the LHM thickness. In addition, the intervals between ODR peaks are almost the same, which is advantage in multiple-channel communications.

We note that there exist intrinsic losses in materials. In order to investigate the losses, we re-calculated the transmission spectra by using transfer matrix method with lossy effective permittivity and permeability. In this case, Eq. (1) should be modified as $\varepsilon_j = \varepsilon_{0j} - \omega_{ep,j}^2/\omega(\omega + i\gamma_{e,j})$ and $\mu_j = \mu_{0j} - \omega_{mp,j}^2/\omega(\omega + i\gamma_{m,j})$.

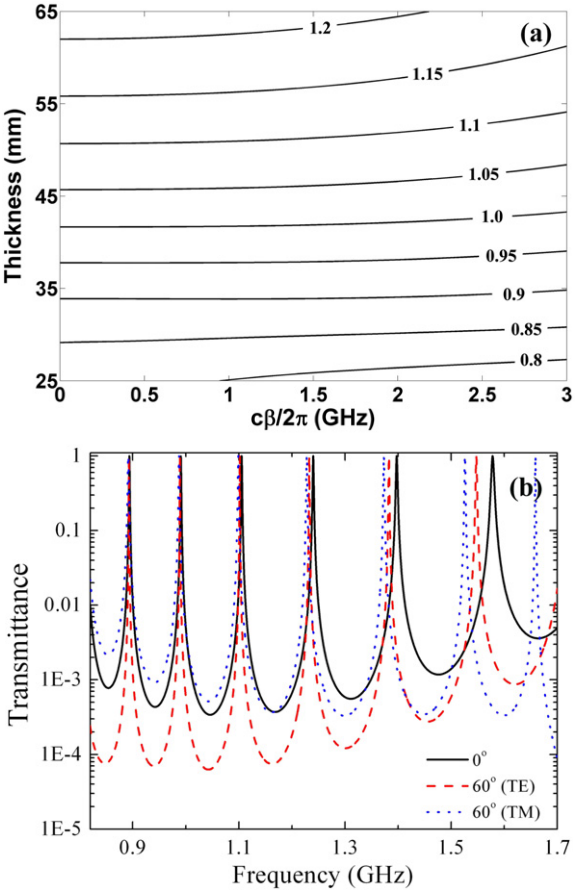

Fig. 5. (Color online.) (a) Contour diagram of resonant frequencies for the AS-TE3 mode. (b) Transmission spectrum of an ELE structure possessing multiple ODRs for both polarizations. The solid, dash and dot lines stand for 0°, 60° (TE), and 60° (TM) incidence. The thicknesses of LHM and ENG are 95.85 and 31.95 mm, respectively.

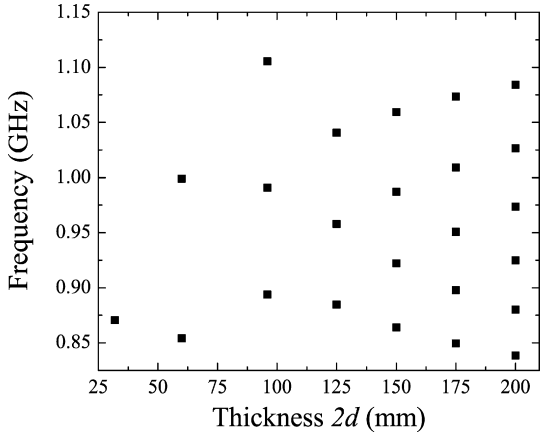

Fig. 6. Distribution on all-polarized ODR peaks with different cavity thicknesses. The quantity $\Delta f/f_0$ is less than 0.005.

The damping coefficients can be evaluated according to Ref. [8]. We find that the realistic losses just decrease the transmission intensity, but the resonant peaks do not shift. For comparison, we also introduced the losses into our photonic crystal structure shown in Ref. [11]. We find that the losses in this sandwich are much lower than that in photonic crystals because of the fewer layers in the former structure.

4. Conclusion

In conclusion, we have found a kind of all-metamaterial-based sandwich structure possessing multiple ODRs. Such structures consist of a left-handed cavity and two single-negative-permittivity walls. These resonances appear because at every incidence angle, the phase matching simultaneously meets in multi-frequencies. Moreover, the angular dependence of TE mode is much smaller than that of TM mode. Finally, multiple ODRs in both polarizations have been practically designed. This multiple channel all-polarized ODRs are important for all-angle applications such as filters and detectors. It may be realized in optical regimes with appropriate optical metamaterials [15,16].

Acknowledgements

This work is supported by the National Natural Science Foundation of China (10674183), National 973 (2004CB719804) Project of China, PhD Degrees Foundation of Ministry of Education of China (20060558068), and Natural Science Foundation of Sun Yat-sen University (2007300003171914).

References

[1] P. Yeh, Optical Waves in Layered Media, Wiley, New York, 1988.
[2] S. Lan, S. Nishikawa, Y. Sugimoto, N. Ikeda, K. Asakawa, H. Ishikawa, Phys. Rev. B 65 (2002) 165208.
[3] H.Y. Lee, T. Yao, J. Appl. Phys. 93 (2003) 819.
[4] H. Shin, M.F. Yanik, S. Fan, R. Zia, M.L. Brongersma, Appl. Phys. Lett. 84 (2004) 4421.
[5] V.G. Veselago, Sov. Phys. Usp. 10 (1968) 509.
[6] A. Grbic, G.V. Eleftheriades, Phys. Rev. Lett. 92 (2004) 117403.
[7] G.V. Eleftheriades, K.G. Balmain, Negative-Refractive Metamaterials: Fundamental Principles and Applications, Wiley, 2005.
[8] R.A. Shelby, D.R. Smith, S. Schultz, Science 292 (2001) 77.
[9] A. Alù, N. Engheta, IEEE Trans. Antennas Propag. 51 (2003) 2558.
[10] Y.H. Chen, J.W. Dong, H.Z. Wang, J. Opt. Soc. Am. B 23 (2006) 776.
[11] Y.H. Chen, J.W. Dong, H.Z. Wang, J. Opt. Soc. Am. B 23 (2006) 2237.
[12] G.S. Guan, H.T. Jiang, H.Q. Li, Y.W. Zhang, H. Chen, S.Y. Zhu, Appl. Phys. Lett. 88 (2006) 211112.
[13] D. Schurig, J.J. Mock, B.J. Justice, S.A. Cummer, J.B. Pendry, A.F. Starr, D.R. Smith, Science 314 (2006) 977.
[14] J.D. Jackson, Classical Electrodynamics, third ed., Wiley, 1999, p. 305.
[15] G. Dolling, M. Wegener, C.M. Soukoulis, S. Linden, Opt. Lett. 32 (2007) 53.
[16] H.K. Yuan, U.K. Chettiar, W. Cai, A.V. Kildishev, A. Boltasseva, V.P. Drachev, V.M. Shalaev, Opt. Express 15 (2007) 1076.